

## How much charm can $\bar{P}ANDA$ produce?

A. Khodjamirian, Ch. Klein, Th. Mannel and Y.-M. Wang

*Theoretische Physik 1, Naturwissenschaftlich-Technische Fakultät,  
Universität Siegen, D-57068 Siegen, Germany*

We consider the production of charmed baryons and mesons in the proton-antiproton binary reactions at the energies of the future  $\bar{P}ANDA$  experiment. To describe these processes in terms of hadronic interaction models, one needs strong couplings of the initial nucleons with the intermediate and final charmed hadrons. Similar couplings enter the models of binary reactions with strange hadrons. For both charmed and strange hadrons we employ the strong couplings and their ratios calculated from QCD light-cone sum rules. In this method finite masses of  $c$  and  $s$  quarks are taken into account. Employing the Kaidalov's quark-gluon string model with Regge poles and adjusting the normalization of the amplitudes in this model to the calculated strong couplings, we estimate the production cross section of charmed hadrons. For  $p\bar{p} \rightarrow \Lambda_c \bar{\Lambda}_c$  it can reach several tens of  $nb$  at  $p_{lab} = 15$  GeV, whereas the cross sections of  $\Sigma_c$  and  $D$  pair production are predicted to be smaller.

# 1 Introduction

There is a vivid interest in the cross-section of charmed hadron production in the proton-antiproton collisions to be measured by the future  $\bar{P}ANDA$  experiment (see, e.g., [1]). The amount of produced charmed mesons and baryons is important for assessing the ability of this experiment to perform flavour-physics oriented studies, such as the measurement of charm-anticharm mixing, the search for  $CP$ -violation in  $D$  decays or the studies of  $\Lambda_c$  decays. A reliable estimate of the  $p\bar{p} \rightarrow \text{charm}$  cross section is however a very difficult task. The main problem is that the projected energy range (with the c.m. energy  $\sqrt{s}$  varying from 2.25 GeV to 5.47 GeV), being reasonably high for the proton-antiproton collisions, is still not far from the threshold of charm-anticharm production. Several models of charm production at these energies can be found in the literature [2, 3, 4, 5, 6, 7, 8, 9, 10], their predictions differing by several orders of magnitude, as emphasized, e.g. in [8]. Especially difficult is to predict the inclusive charm-anticharm cross section in the situation where not many exclusive channels are open. Hence, it is more realistic to assess the exclusive production of baryons or mesons, such as  $p\bar{p} \rightarrow \Lambda_c \bar{\Lambda}_c, \bar{D}D$ . A successful model of strange-hadron pair production in  $p\bar{p}$  collisions, which was measured at similar energies, can serve as a useful tool, provided there is a reliable way to replace the model parameters of strange hadrons by the ones for charmed hadrons. The key parameters in many hadronic models of these processes are the strong couplings of strange or charmed baryons with mesons and nucleons. To relate them, the  $SU(4)_{fl}$ -symmetry is frequently used in the literature. Note however, that it is difficult to justify this symmetry in QCD, due to the large mass difference of the  $c$ - and  $s$ -quarks,  $m_c - m_s \gg \Lambda_{QCD}$ .

In this paper we employ the strong baryon-meson couplings of charmed and strange hadrons calculated from QCD light-cone sum rules (LCSR), where finite masses of  $c$  and  $s$  quark are taken into account. Recently, we calculated [11] the charmed baryon strong couplings with a charmed meson and a nucleon. In addition to these results, here we obtain the corresponding strong couplings of strange hadrons. The nonperturbative inputs in the LCSR method are the universal nucleon distribution amplitudes (DA's). Hence, the extension of our calculation from charmed to strange hadrons is straightforward and is reduced to a replacement of the virtual  $c$ -quark by an  $s$ -quark in the underlying correlation functions. In what follows, we also employ the ratios of calculated strong couplings which are predicted from LCSR with smaller uncertainties than the individual couplings.

The results for the strong couplings presented here can be used in various models of exclusive charm and strange hadron production. As an application of our results, we use the quark-gluon string (QGS) model of binary reactions developed by Kaidalov and his collaborators [12, 13, 14, 15]. One version of this model was already applied in [2] to estimate the charm production cross section in proton-antiproton collisions. We refine this model by introducing the helicity amplitudes and adjusting the two independent strong couplings to the LCSR estimates.

In what follows, in Sect. 2 we present the LCSR results for strong couplings of charmed and strange hadrons. In Sect. 3 we demonstrate how the QGS model works for relatively

simple processes of meson pair production and trace the relation between the model parameters and strong couplings in QCD. In Sect. 4 we use the QGS model for  $p\bar{p}$  binary reactions with charmed and strange hadrons, employing the strong couplings from LCSR and predict the charm production cross sections. Sect. 5 contains the concluding discussion. The two appendices contain: (A) the formulae for helicity amplitudes and (B) the derivation of the absorption factor in  $p\bar{p}$  binary processes.

## 2 Strong couplings from QCD light-cone sum rules

The strong couplings of the  $\Lambda_c$ -baryon with the nucleon and  $D$  or  $D^*$  meson are formally defined as the following hadronic matrix elements:

$$\begin{aligned}\langle \Lambda_c(P-q) | D(-q) N(P) \rangle &= g_{\Lambda_c N D} \bar{u}_{\Lambda_c}(P-q) i\gamma_5 u_N(P), \\ \langle \Lambda_c(P-q) | D^*(-q) N(P) \rangle &= \bar{u}_{\Lambda_c}(P-q) \left( g_{\Lambda_c N D^*}^V \not{\epsilon} + i \frac{g_{\Lambda_c N D^*}^T}{m_{\Lambda_c} + m_N} \sigma_{\mu\nu} \epsilon^\mu q^\nu \right) u_N(P).\end{aligned}\quad (1)$$

Note that the above couplings are defined in [11] as residues at the  $D^{(*)}$  and  $\Lambda_c$  poles in double dispersion relations for the correlation functions with on-shell nucleon state, hence all three hadrons are on their mass-shell. The same definitions are valid for the  $\Sigma_c$ -baryon couplings as well as for the corresponding strange hadrons with the following replacements:  $\Lambda_c(\Sigma_c) \rightarrow \Lambda(\Sigma)$  and  $D^{(*)} \rightarrow K^{(*)}$  in the above.

The  $\Lambda_c N D^{(*)}$  and  $\Sigma_c N D^{(*)}$  strong couplings were calculated from LCSR in [11], where one can find the detailed description of the sum rule derivation. The results for the strong couplings which will be used in this paper are collected in Table 1. Note that in [11] two different interpolating currents for  $\Lambda_c$  and  $\Sigma_c$  baryons were used. With the procedure of eliminating the negative parity baryons suggested in that paper, the results agree within the uncertainties. In this paper we will only use the strong couplings obtained for the pseudoscalar interpolating current for  $\Lambda_{(c)}$  and Ioffe current for  $\Sigma_{(c)}$ , respectively, because the sum rules in these cases have a comparatively lower background of higher states. In Table 1 also the ratios of strong couplings obtained from LCSR are presented, generally they have smaller estimated uncertainties, because of the common inputs used in the sum rules.

Turning to strange hadrons, we employ the same LCSR method as in [16, 17] and, replacing  $c$ -quark with the  $s$ -quark in the correlation function, calculate the  $\Lambda N K^{(*)}$  and  $\Sigma N K^*$  couplings. The inputs used in LCSR consist of universal nucleon DA's which are taken from [18] and explained in detail in [11]. In particular we use for the virtual  $c$  quark in the correlation function the value  $m_c(m_c) = 1.28 \pm 0.03$  GeV. The flavour-specific input parameters which we adopt here for the sum rules involving strange hadrons are: the strange quark mass  $m_s(2 \text{ GeV}) = 98 \pm 16$  MeV and the renormalization scale  $\mu_s = 1.0 \pm 0.2$  GeV. Furthermore, one and the same range  $M^2 = 2.0 \pm 0.5$  GeV<sup>2</sup> of the Borel parameter in the  $\Sigma$  and  $\Lambda$  channels is adopted, whereas for the  $K^*$  channel we use  $\tilde{M}^2 = 1.0 \pm 0.5$  GeV<sup>2</sup>. The threshold parameter in the LCSR for  $\Lambda(\Sigma)$  strong couplings is taken  $s_0 = 2.55 \pm 0.10$  GeV<sup>2</sup> ( $s_0 = 2.75 \pm 0.10$  GeV<sup>2</sup>). The criteria of

Strong coupling (charmed)	LCSR estimate	Strong coupling (strange)	LCSR estimate	Ratio of couplings ( $\frac{\text{charmed}}{\text{strange}}$ )	LCSR estimate
$g_{\Lambda_c ND}$	$10.7^{+5.3}_{-4.3}$	$g_{\Lambda NK}$	$7.3^{+2.6}_{-2.8}$	$\frac{g_{\Lambda_c ND}}{g_{\Lambda NK}}$	$1.47^{+0.58}_{-0.44}$
$g_{\Lambda_c ND}^V$	$-5.8^{+2.1}_{-2.5}$	$g_{\Lambda NK}^V$	$-6.1^{+2.1}_{-2.0}$	$\frac{g_{\Lambda_c ND}^V}{g_{\Lambda NK}^V}$	$0.95^{+0.35}_{-0.28}$
$g_{\Lambda_c ND}^T$	$3.6^{+2.9}_{-1.8}$	$g_{\Lambda NK}^T$	$12.8^{+5.8}_{-5.2}$		
$\frac{g_{\Lambda_c ND}^T}{g_{\Lambda_c ND}^V}$	$-0.63^{+0.16}_{-0.28}$	$\frac{g_{\Lambda NK}^T}{g_{\Lambda NK}^V}$	$-2.1^{+0.5}_{-0.6}$		
$g_{\Sigma_c ND}$	$1.3^{+1.0}_{-0.9}$	$g_{\Sigma NK}$	$1.1^{+0.6}_{-0.5}$		
$g_{\Sigma_c ND}^V$	$1.0^{+1.3}_{-0.6}$	$g_{\Sigma NK}^V$	$1.7^{+0.9}_{-0.8}$	$\frac{g_{\Sigma_c ND}^V}{g_{\Sigma NK}^V}$	$0.56^{+0.42}_{-0.20}$
$g_{\Sigma_c ND}^T$	$2.1^{+1.9}_{-1.0}$	$g_{\Sigma NK}^T$	$3.6^{+1.5}_{-1.2}$		
$\frac{g_{\Sigma_c ND}^T}{g_{\Sigma_c ND}^V}$	$2.1 \pm 0.5$	$\frac{g_{\Sigma NK}^T}{g_{\Sigma NK}^V}$	$2.1^{+0.6}_{-0.3}$		

Table 1: Numerical results for the strong couplings of charmed [11] and strange baryons and their ratios obtained from LCSR with nucleon DA's.

choosing the input parameters and the quark-hadron duality ansatz in LCSR are the same as the ones used and discussed in [11]. The two-point QCD sum rules for the decay constants of  $\Lambda$  and  $\Sigma$  baryons with pseudoscalar and Ioffe currents respectively, are taken from [19]. Using the same definitions and notation as for the decay constants of charmed baryons in [11]), we obtain:

$$\lambda_{\Lambda}^{(P)} = (0.87^{+0.23}_{-0.13}) \times 10^{-2} \text{ GeV}^2, \quad \lambda_{\Sigma}^{(T)} = (2.6^{+0.3}_{-0.2}) \times 10^{-2} \text{ GeV}^2. \quad (2)$$

The resulting estimates of the strange baryon strong couplings and their ratios obtained from LCSR are presented in Table 1. Note that  $\Lambda_c$  and  $\Sigma_c$  belong to different  $SU(3)$  multiplets (as opposed to  $\Lambda$  and  $\Sigma$ ), and this circumstance explains a substantial difference between the ratios of tensor and vector strong couplings for these baryons.

In the literature (see e.g., [3]), the strong couplings of charmed hadrons are estimated assuming  $SU(4)_{fl}$  symmetry and equating dimensionless couplings, for example, assuming  $g_{\Lambda_c ND}^{V(T)} \simeq g_{\Lambda NK}^{V(T)}$ . Such symmetry relations are difficult to justify from the point of view of QCD. Indeed, because of the large mass difference of  $c$  and  $s$  quarks, the kinematical factors: masses and four-momenta entering the complete hadronic matrix elements differ significantly. In our approach we are not relying on any form of the  $SU(4)_{fl}$  symmetry. Still, it is interesting to compare the strong couplings for the charmed and

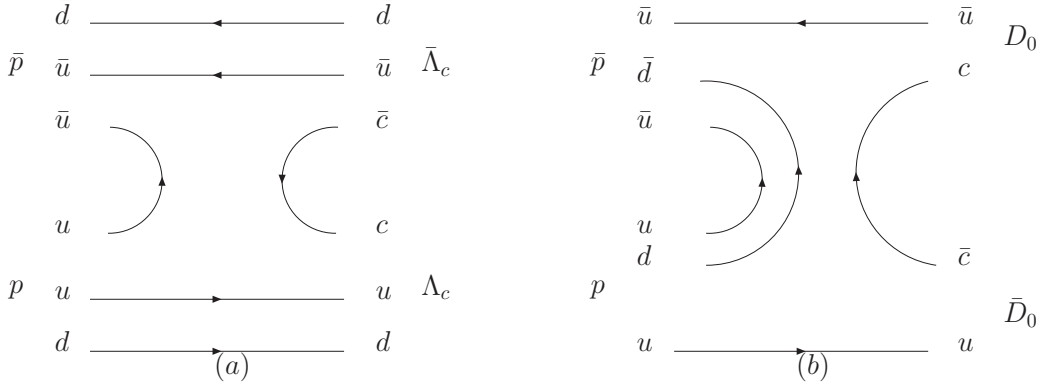


Figure 1: *The planar diagram of charmed baryon (a) and meson (b) pair production in  $p\bar{p}$  collisions.*

strange baryons obtained from LCSR and collected in Table 1. We find that the values of the dimensionless  $g^V$  couplings are in the same ballpark, whereas there is a significant difference between  $g_{\Lambda NK}^T$  and  $g_{\Lambda_c ND}^T$ . The strange baryon couplings were also calculated with the Nijmegen potential model [20] of low-energy scattering, assuming  $SU(3)_{fl}$ -symmetry. Expressed in terms of the dimensionless  $g$ -couplings defined in (1) the results of [20] with their sign conventions are:

$$\begin{aligned}
 g_{\Lambda NK} &= 13.4 \div 17.5, & g_{\Lambda NK}^V &= -(4.3 \div 6.1), & g_{\Lambda NK}^T &= 12.4 \div 16.3, \\
 g_{\Sigma NK} &= -(4.1 \div 5.3), & g_{\Sigma NK}^V &= -(2.4 \div 3.5), & g_{\Sigma NK}^T &= -(1.3 \div 4.6).
 \end{aligned}
 \quad (3)$$

Comparing with our predictions for the strange-baryon couplings given in Table 1, we observe an agreement for vector-meson couplings within uncertainties. Also the convention-independent relative signs of  $T$  and  $V$  couplings agree. Meanwhile, the LCSR predictions for  $g_{\Lambda NK}$  and  $g_{\Sigma NK}$  are systematically lower than the intervals for these couplings obtained in the potential model.

### 3 The QGS model for meson pair production

In the QGS model, the amplitudes of binary reactions, such as  $p\bar{p} \rightarrow \Lambda_c \bar{\Lambda}_c$  or  $p\bar{p} \rightarrow \bar{D}D$ , are described by planar diagrams depicted in Fig. 1. These diagrams have a dual interpretation. From the  $s$ -channel point of view, annihilation of the slow  $u\bar{u}$  or  $d\bar{d}$  pair from the initial proton and antiproton is followed by a creation of the  $c\bar{c}$ -pair. The spectator quarks and antiquarks from the initial proton and antiproton coalesce with the created quark and antiquark to form the final state charmed hadrons. The intermediate state in  $s$ -channel represents a sort of a diquark-antidiquark (Fig.1 a) or quark-antiquark (Fig.1 b) string. On the other hand, in the  $t$ -channel a virtual hadronic state with the quantum numbers of a charmed meson or baryon is exchanged. In the  $s \gg |t|$  limit, this exchange is described by the dominant Regge pole. For instance, the amplitude of  $p\bar{p} \rightarrow \Lambda_c \bar{\Lambda}_c$  is approximated by the (degenerate)  $D^*, D^{**}$  Regge-trajectory

$\alpha_{D^*}(t) = \alpha_{D^*}(0) + \alpha'_{D^*}t$  (we use the linear approximation). The QGS-model parameters are obtained [2, 12, 13, 14] using the quark-parton description of the  $s$ -channel planar diagram. Replacing the  $c$ -quark by  $s$ -quark in the planar diagrams of Fig. 1 we reproduce the QGS model for the production of strange baryons and mesons. The strange-hadron pair production cross section in  $p\bar{p}$  collisions calculated in this model [2] agrees well with the experimental data. Importantly, there is a strong flavour dependence of the binary reactions in QGS model, encoded in the slopes and intercepts of the Regge trajectories as well as in the scale factors  $s_0$  entering the Regge amplitudes. The relative suppression of the charmed hadron production corresponds, in terms of the  $s$ -channel picture, to a comparatively smaller probability to create a heavy quark-antiquark pair within the intermediate string.

To discuss the QGS model in more detail, we first consider a relatively simple binary reaction involving no spins or helicities:  $\pi^+\pi^- \rightarrow M\bar{M}$ , with pseudoscalar mesons ( $M = \pi^0, K^+, \bar{D}^0$ ) of various flavours in the final state and with isospin and/or flavour exchange in  $t$ -channel. The planar diagram of this process is shown in Fig. 2. At large  $s$  and small  $|t| \ll s$ , the scattering amplitude is written [2] in the following Regge-pole form:

$$T^{(\pi^+\pi^- \rightarrow M\bar{M})}(s, t) = g^{(\pi M)}(t) \frac{s}{\bar{s}} \left( \frac{s}{s_0^{\pi M}} \right)^{\alpha_R(t)-1}, \quad (4)$$

where  $\bar{s} = 1 \text{ GeV}^2$  is a universal dimensional factor and the energy dependence is determined by the Regge trajectory  $\alpha_R(t)$  with the corresponding quantum numbers ( $R = \rho(a_2), K^{*(**)}, D^{*(**)}$ ). In the above,  $g^{\pi M}(t)$  is the residue function of the momentum transfer squared. In the QGS model [2] the  $\Gamma$ -function dependence inspired by Veneziano duality is adopted:

$$g^{(\pi M)}(t) = C^{(\pi M)} g_0^2 \Gamma(1 - \alpha_R(t)). \quad (5)$$

The coefficient  $C^{(\pi M)}$  is equal to the number of planar diagrams.

The amplitude (4) for  $\pi^+\pi^- \rightarrow \pi^0\pi^0$  is determined by the  $\rho(a_2)$ -trajectory:

$$\alpha_R(t) = \alpha_\rho(t) = \alpha_\rho(0) + \alpha'_\rho t. \quad (6)$$

In this case  $C^{(\pi\pi)} = 2$ , and the numerical values of the intercept  $\alpha_\rho(0)$  and slope  $\alpha'_\rho$  taken from [2] are presented in Table 2.

The universal parameter  $g_0$  in QGS model can be related to the  $\rho\pi\pi$  strong coupling defined as:

$$\langle \pi^-(p_1)\pi^0(p_2) | \rho^-(p_1 + p_2) \rangle = g_{\rho\pi\pi} \epsilon_\mu^{(\rho)}(p_2 - p_1)^\mu, \quad (7)$$

where  $\epsilon^{(\rho)}$  is the polarization 4-vector of  $\rho$ -meson. The numerical value  $g_{\rho\pi\pi} \simeq 6.0$  with a negligible error is then obtained from the measured [21] width:

$$\Gamma(\rho \rightarrow \pi\pi) = \frac{g_{\rho\pi\pi}^2}{6\pi m_\rho^2} (p_{\rho\pi\pi}^*)^3, \quad (8)$$

where  $p_{\rho\pi\pi}^* = (m_\rho/2)\sqrt{1 - 4m_\pi^2/m_\rho^2}$  is the 3-momentum of the pions in the rest frame of the  $\rho$ . Combining the product of couplings defined in (7) with the  $\rho$  propagator

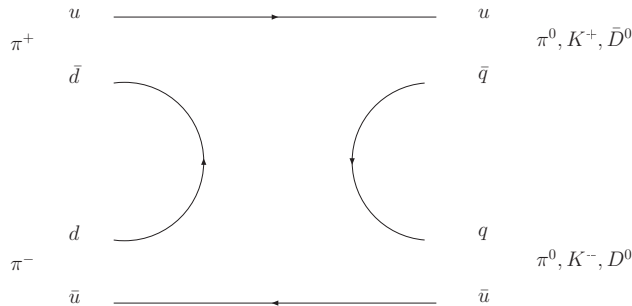


Figure 2: The planar diagram of  $\pi^+\pi^- \rightarrow M\bar{M}$  ( $q = u, s, c$  and  $M = \pi^0, K^+, \bar{D}^0$ ). An additional diagram with  $u \leftrightarrow d$  contributes to the  $\pi^0\pi^0$ -production.

process	Regge pole	intercept $\alpha_R(0)$	slope $\alpha'_R(\text{GeV}^{-2})$	scale param. $s_0^{\pi M}(\text{GeV}^2)$	$C^{(\pi M)}$
$\pi^+\pi^- \rightarrow \pi^0\pi^0$	$\rho$	0.46	0.9	1.0	2
$\pi^+\pi^- \rightarrow K^+K^-$	$K^*$	0.32	0.85	1.25	1
$\pi^+\pi^- \rightarrow D^0\bar{D}^0$	$D^*$	-0.86	0.5	3.55	1

Table 2: Parameters of Regge trajectories [2] involved in the  $\pi^+\pi^- \rightarrow M\bar{M}$ .

(neglecting the width) we calculate the  $\pi^+\pi^- \rightarrow \pi^0\pi^0$  scattering amplitude in a form of a Feynman diagram with an “elementary”  $\rho$ -meson exchange in  $t$ -channel. The result is

$$T_{diag}^{(\pi^+\pi^- \rightarrow \pi^0\pi^0)}(s, t) = g_{\rho\pi\pi}^2 \frac{2s + t - 4m_\pi^2}{m_\rho^2 - t}. \quad (9)$$

At  $s \gg |t|, m_{\pi, \rho}^2$  the above amplitude correctly reproduces the expected  $s^J$  asymptotics, where  $J = 1$  is the spin of the vector meson exchanged in  $t$ -channel. The Regge amplitude (4), being analytically continued in the Mandelstam  $\{s, t\}$  plane to  $t \sim m_\rho^2$  has to reproduce the Feynman diagram expression (9) at  $s \gg m_\pi^2, |t|$ . Substituting (5) in (4) and expanding the  $\Gamma$ -function near  $t = m_\rho^2$  where  $\alpha_\rho(m_\rho^2) = 1$  we obtain a pole in the variable  $t$ :

$$\Gamma(1 - \alpha_\rho(t)) \simeq \frac{1}{\alpha'_\rho(m_\rho^2 - t)}, \quad (10)$$

which corresponds to the  $\rho$ -propagator pole in (9). Comparing the residues of the amplitudes (4) and (9) at large  $s$ , we obtain

$$\frac{C^{(\pi\rho)} g_0^2}{\alpha'_\rho \bar{s}} = 2g_{\rho\pi\pi}^2. \quad (11)$$

Numerically, the above equation at the values  $\alpha'_\rho = 0.9$  and  $g_0^2/(4\pi) = 2.7$  adopted in [2] correctly reproduces the experimental value of  $g_{\rho\pi\pi}$ .

Repeating the same comparison for the binary reaction  $\pi^+\pi^- \rightarrow K^+K^-$  with the strangeness-exchange in the  $t$ -channel, we replace the  $\rho$  trajectory by the  $K^*$  trajectory in the Regge-pole amplitude (4). The corresponding parameters of GGS model are presented in Table 2. Note that the  $SU(3)_{fl}$  violation in this model (i.e. the effect of a heavier  $s$ -quark) is reflected in the parameters of Regge trajectory, and also in the flavour-dependent normalization scale  $s_0^{\pi K}$ , introduced in QGS approach. We then compare the residue function near the pole at  $t = m_{K^*}^2$  with the diagram containing the  $K^*$  propagator and the  $K^*K\pi$  strong couplings. This diagram yields an expression similar to (9):

$$T_{diag}^{(\pi^+\pi^- \rightarrow K^+K^-)}(s, t) = \frac{g_{K^*K\pi}^2}{m_{K^*}^2 - t} \left( 2s + t - 2(m_\pi^2 + m_K^2) + \frac{(m_K^2 - m_\pi^2)^2}{m_{K^*}^2} \right), \quad (12)$$

with the same large  $s$  asymptotic behavior. The relation analogous to (11) yields  $g_{K^*K\pi} = 4.5$  for the  $K^{*0}K^+\pi^-$  strong coupling. This is very close to the value extracted from the  $K^* \rightarrow K\pi$  width [21].

Turning to the charmed meson production in the two-pion collisions, we consider the amplitude (4) with the  $D^*$  Regge-trajectory:

$$T^{(\pi^+\pi^- \rightarrow D^0\bar{D}^0)}(s, t) = g_0^2 \Gamma(1 - \alpha_{D^*}(t)) \frac{s}{\bar{s}} \left( \frac{s}{s_0^{\pi D}} \right)^{\alpha_{D^*}(t)-1}. \quad (13)$$

In the QGS approach, the flavour-dependence of the amplitude is reflected by the substantial differences between the slope parameters of  $D^*$  and  $\rho(K^*)$  trajectories on one hand, and between the scale factors  $s_0^{\pi D}$  and  $s_0^{\pi\pi(\pi K)}$  on the other hand, as can be seen from Table 2. Hence as we already mentioned, there is no  $SU(4)_{fl}$  symmetry in this model. Still there remains an important question if the universal value of  $g_0^2$  can be used also in the charm production amplitude. The  $D^*D\pi$  strong coupling is defined as <sup>1</sup>

$$\langle \pi^-(p_1) D^0(p_2) | D^{*-}(p_1 + p_2) \rangle = g_{D^*D\pi} \epsilon_\mu^{(D^*)} (p_2 - p_1)^\mu, \quad (14)$$

and the ‘‘elementary’’  $D^*$ -exchange diagram yields the same expression as in (12), where  $K \rightarrow D$  and  $K^* \rightarrow D^*$  have to be replaced. Continuing the Regge amplitude to  $t = m_{D^*}^2$  and comparing with the large  $s$  limit of the  $D^*$ -exchange (12), we obtain:

$$\frac{g_0^2}{\alpha'_{D^*} \bar{s}} = 2g_{D^*D\pi}^2. \quad (15)$$

Substituting the slope of the  $D^*$  trajectory and using the universal value  $g_0^2$  of the QGS model [2] we obtain<sup>2</sup>:  $g_{D^*D\pi} = 5.8$ . Interestingly, this value is close to the interval estimated from QCD LCSR in [22] taking into account the gluon radiative corrections [23]:  $[g_{D^*D\pi}]_{\text{LCSR}} = 5.0 \pm 1.75$ . The only existing measurement of the total  $D^*$  width combined with the branching fraction yields a larger result:  $[g_{D^*D\pi}]_{\text{exp.}} = 8.95 \pm 0.15 \pm 0.95$  [24]. We conclude that the  $D^*$  trajectory slope adopted in QGS model is consistent with the LCSR estimates of the  $D^*D\pi$  strong coupling.

<sup>1</sup> Note that  $2g_{D^*D\pi}$  is equal to the  $D^*D\pi$  coupling defined in [22].

<sup>2</sup> Our estimate differs from the smaller value quoted in [15] and based on the same model. Note that in this earlier paper a larger value of the slope  $\alpha'_{D^*} = 0.64$  was used.



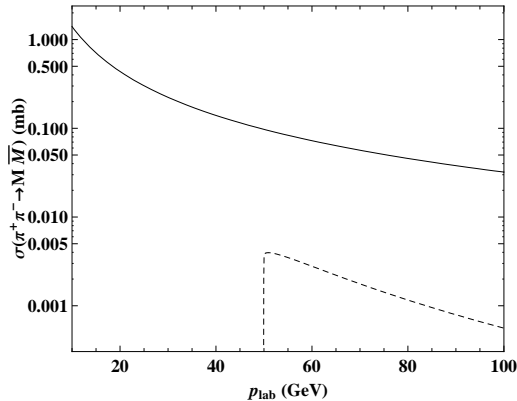


Figure 3: Dependence of the cross sections of  $\pi^+\pi^- \rightarrow K^+K^-$  (solid) and  $\pi^+\pi^- \rightarrow D^0\bar{D}^0$  (dashed) on  $p_{\text{lab}}$  in QGS model.

Note that one of the inputs used to determine the  $D^*$  trajectory of in QGS model is the Regge trajectory of  $J/\psi$ , taken in [2] as:

$$\alpha_\psi(t) = -2.18 + 0.33t, \quad (16)$$

and supported by the QGS model analysis of inclusive charm production. Here one can mention the estimate of the intercept  $\alpha_\psi(0)$  obtained in [25], where a four-point correlation function of heavy-quark-currents was first calculated using OPE in terms of loop diagram and vacuum condensates and then, via optical theorem, related to the photon-heavy meson scattering cross section taken in the Regge form. The comparison of two representations of the correlation function yields  $\alpha_\psi(0) = -(2 \sim 3)$ , consistent with (16). Note that the perturbative loop approximation in [25] yields  $\alpha_\psi(0) = 0$ , hence the estimated value of this parameter is entirely determined by nonperturbative (gluon- and quark-condensate) effects.

To illustrate the QGS model for meson pair production, in Fig. 3 we present the cross sections of the processes discussed in this section. According to our definition of the scattering amplitude, the differential cross section is:

$$\frac{d\sigma}{dt}(\pi^+\pi^- \rightarrow M\bar{M}) = \frac{|T^{(\pi^+\pi^- \rightarrow M\bar{M})}(s, t)|^2}{16\pi s(s - 4m_\pi^2)}, \quad (17)$$

where we substitute the Regge-pole amplitude (4) for  $M = K, D$  and integrate over  $|t|$  from the kinematically allowed minimal  $|t_0|$  to  $|t_0| + \Delta$ . Here we choose for definiteness  $\Delta = 0.6 \text{ GeV}^2$ , so that  $|t|$  remains much smaller than  $s$  and hence the Regge-pole description is applicable. Hereafter we refrain from predicting total cross sections, because at large  $|t| \sim s$  the behavior of the scattering amplitudes is governed by mechanisms other than a simple Regge-pole model. Still, differential cross sections rapidly decrease with  $|t|$ , hence, our results for the integrated cross sections provide an order-of-magnitude estimate also for the total cross sections. As we can see from Fig. 3, the charmed meson production cross section is strongly suppressed with respect to the strange-meson one.

## 4 $p\bar{p}$ - production of charmed and strange hadrons

The QGS model of the charmed baryon-pair production in  $p\bar{p}$  collision is described by the planar diagram in Fig. 1a. This amplitude, similar to  $\pi\pi \rightarrow D\bar{D}$ , is approximated by the  $D^*$  Regge-trajectory. The amplitude of  $p\bar{p} \rightarrow \Lambda_c\bar{\Lambda}_c$  presented in [2] has a helicity-averaged form

$$|T^{(p\bar{p} \rightarrow \Lambda_c\bar{\Lambda}_c)}(s, t)| = g^{(p\Lambda_c)}(t) \frac{s}{s_0} \left( \frac{s}{s_0^{p\Lambda_c}} \right)^{\alpha_{D^*}(t)-1}, \quad (18)$$

where the residue function  $g^{(p\Lambda_c)}(t) = C^{p\Lambda_c} g_0^2 \Gamma(1 - \alpha_{D^*}(t))$  contains the same universal coupling  $g_0^2$ . Importantly, the scale factor  $s_0^{p\Lambda_c}$  obtained following [2] (see Table 3) is not equal to  $s_0^{\pi D}$ , reflecting the difference between baryon and meson production in this model.

Here we consider a more elaborated version of the QGS model for this process with the helicity amplitudes (see App. A). The differential cross section has the following expression

$$\begin{aligned} \frac{d\sigma}{dt}(p\bar{p} \rightarrow \Lambda_c\bar{\Lambda}_c) &= \frac{1}{32\pi s(s - 4m_p^2)} \left[ |H(+++, ++)|^2 + 2|H(+-, ++)|^2 \right. \\ &\left. + 2|H(+++, -+)|^2 + |H(--, ++)|^2 + |H(-+, -+)|^2 + |H(+-, -+)|^2 \right], \quad (19) \end{aligned}$$

where in the helicity amplitudes  $H(\lambda_1\lambda_2; \lambda_3\lambda_4)$  the notation  $\lambda_{1,2}, (\lambda_{3,4})$  denotes the helicities of the proton and antiproton ( $\Lambda_c$  and  $\bar{\Lambda}_c$ ), respectively. The  $s, t$  dependence of the amplitudes is not shown for brevity. At fixed  $s$ , the region of the momentum transfer squared  $t$  is given by  $t_1 < t < t_0$ , where:

$$t_{0(1)} = m_p^2 + m_{\Lambda_c}^2 - \frac{s}{2} + (-)\frac{1}{2}\sqrt{(s - 4m_p^2)(s - 4m_{\Lambda_c}^2)}. \quad (20)$$

We assume that each helicity amplitude has the Regge form (18). The residue functions are fixed by continuing these Regge amplitudes to the point  $t = m_{D^*}^2$  and matching them to the helicity amplitudes of  $p\bar{p} \rightarrow \Lambda_c\bar{\Lambda}_c$  with an ‘‘elementary’’  $D^*$  exchange. The latter are given in App. A. (see eq.(31)) and contain two independent strong  $\Lambda_c D^* N$  couplings defined in (1), so that the coupling  $g_{\Lambda_c N D^*}^V$  ( $g_{\Lambda_c N D^*}^T$ ) enters the helicity-nonflip (-flip) amplitudes. We arrive at the following expression for the cross section:

$$\begin{aligned} \frac{d\sigma}{dt}(p\bar{p} \rightarrow \Lambda_c\bar{\Lambda}_c) &= \frac{C_A^{(p\bar{p} \rightarrow \Lambda_c\bar{\Lambda}_c)}(s, t)}{4\pi s(s - 4m_p^2)} |R_{D^*}(s, t)|^2 \\ &\times \left( |g_{\Lambda_c N D^*}^V|^2 + \frac{|t|}{(m_{\Lambda_c} + m_N)^2} |g_{\Lambda_c N D^*}^T|^2 \right)^2, \quad (21) \end{aligned}$$

where the function

$$R_{D^*}(s, t) = \alpha'_{D^*} \Gamma(1 - \alpha_{D^*}(t)) s \left( \frac{s}{s_0} \right)^{\alpha_{D^*}(t)-1} \quad (22)$$

is determined by the Regge-pole parameters. As opposed to  $\pi\pi \rightarrow M\bar{M}$ , where we used the original QGS model with the universal normalization parameter  $g_0^2$ , there is now a more subtle substructure of the Regge amplitudes with the strong couplings determining the helicity-flip and helicity-nonflip amplitudes. Furthermore, we modified the above cross section with respect to (19) by multiplying it with the so called absorption factor  $C_A^{(p\bar{p} \rightarrow \Lambda_c \bar{\Lambda}_c)}$  which is included following [2]. This factor derived in App. B takes into account the initial- and final-state rescattering of the baryons and antibaryons and suppresses the cross sections.

The related processes of charmed baryon production:  $p\bar{p} \rightarrow \Sigma_c \bar{\Lambda}_c$  and  $p\bar{p} \rightarrow \Sigma_c \bar{\Sigma}_c$ , have a similar description in QGS model, in particular, they are also dominated by the same  $D^*$  Regge-pole exchange. Their cross sections depend on the combinations of couplings  $g_{\Sigma_c ND^*}^{V,T}$  and  $g_{\Lambda_c ND^*}^{V,T}$ . The corresponding expressions in terms of helicity amplitudes have minor differences with respect to (19) which we will not discuss here for brevity. The numerical analysis yields a substantial suppression of the  $\Sigma_c$  production versus  $\Lambda_c$  production, due to the difference in the strong couplings inferred from LCSR. This suppression will be discussed below in more detail.

The charmed-meson production,  $p\bar{p} \rightarrow \bar{D}D$ , is described in QGS model by the planar diagram depicted in Fig. 1b. In this case the  $t$ -channel exchange involves  $\Lambda_c$  and  $\Sigma_c$  Regge-trajectories. Their parameters presented in Table 3 are assumed equal. However according to our predictions, the strong couplings of these baryons to mesons and nucleons quite differ from each other, hence there is a significant difference between the cross sections of charged and neutral charmed meson-pair production. Indeed, in the planar diagram model, the process  $p\bar{p} \rightarrow D^- D^+$  can only be mediated by the  $\Sigma_c^{++}$  exchange in  $t$ -channel, whereas in  $p\bar{p} \rightarrow \bar{D}^0 D^0$  both trajectories  $\Lambda_c$  and  $\Sigma_c^+$  enter the amplitude. Note that this is a characteristic feature of the planar diagram mechanism. Inelastic scattering in the final state ( $D^0 \bar{D}^0 \rightarrow D^+ D^-$ ) due to nonplanar diagrams can enhance  $D^+ D^-$  production cross section. Moreover, in a model where these processes are mediated by intermediate charmonium states in  $s$ -channel,  $p\bar{p} \rightarrow \{\bar{c}c\} \rightarrow D\bar{D}$ , there is no correlation between the flavours of initial and final hadrons, so that both charged and neutral  $D$  mesons are produced with equal rates. Such a model may indeed work as an additional mechanism for charmed meson-pair production slightly above the threshold, (see e.g., [10]) but the resulting cross section is much smaller than the one generated by  $t$ -channel exchanges. Let us also mention that, according to the model [9] based on the baryon-antibaryon potential, the initial state inelastic interaction could significantly enhance the  $D^+ D^-$  production cross section in the near-threshold region. Therefore, the charged charmed meson cross section can serve as a useful check of different charm-production models.

The decomposition in the helicity amplitudes in  $p\bar{p} \rightarrow \bar{D}D$  is simpler than for the baryon-pair production because only the helicities of the initial proton and antiproton are involved. For the  $\bar{D}^0 D^0$  production we follow the same method of matching the Regge-pole amplitude to the “elementary”  $\Lambda_c$ -exchange at  $t = m_{\Lambda_c}^2$  and obtain the cross

process	Regge pole	$\alpha_R(0)$	$\alpha'_R(\text{GeV}^{-2})$	$s_0^{pH}(\text{GeV}^2)$
$p\bar{p} \rightarrow \Lambda_c \bar{\Lambda}_c, \Sigma_c \bar{\Sigma}_c$	$D^*$	-0.86	0.5	5.76
$p\bar{p} \rightarrow \Lambda \bar{\Lambda}, \Sigma \bar{\Sigma}$	$K^*$	0.32	0.85	2.43
$p\bar{p} \rightarrow D^0 \bar{D}^0$	$\Lambda_c, \Sigma_c$	-1.82	0.5	3.30
$p\bar{p} \rightarrow D^+ D^-$	$\Sigma_c$			
$p\bar{p} \rightarrow K^+ K^-$	$\Lambda, \Sigma$	-0.64	0.85	1.93
$p\bar{p} \rightarrow K^0 K^0$	$\Sigma$			

Table 3: *Parameters of the Regge trajectories determining the  $p\bar{p}$  amplitudes of charmed and strange hadron-pair production in QGS model [2].*

section:

$$\frac{d\sigma}{dt}(p\bar{p} \rightarrow \bar{D}^0 D^0) = \frac{C_A^{(p\bar{p} \rightarrow \bar{D}^0 D^0)}(s, t)}{32\pi s(s - 4m_p^2)} |R_{\Lambda_c}(s, t)|^2 (m_{\Lambda_c}^2 - t) |g_{\Lambda_c ND}|^4, \quad (23)$$

where

$$R_{\Lambda_c}(s, t) = \alpha'_{\Lambda_c} \Gamma\left(\frac{1}{2} - \alpha_{\Lambda_c}(t)\right) \sqrt{s} \left(\frac{s}{s_0^{pD}}\right)^{\alpha_{\Lambda_c}(t)-1/2}, \quad (24)$$

and the  $\Sigma_c$  exchange contribution is neglected due to much smaller couplings. The absorption factor  $C_A^{(p\bar{p} \rightarrow \bar{D}^0 D^0)}$  in the above cross section has a form similar to the one in (21).

Turning to the numerical analysis of the cross sections we notice that LCSR predictions for strong couplings have a typical error of  $\sim 50\%$ , hence their fourth powers in the cross sections introduce large uncertainties. This mainly concerns the  $g^V$ -couplings. The ratios  $g^T/g^V$  are predicted from LCSR with much smaller uncertainties and moreover, the helicity-flip contributions to the cross sections proportional to  $g^T$ -couplings are kinematically suppressed at small  $t$ .

In order to decrease the uncertainty of the predicted cross sections for charmed hadrons we consider also the strange hadron pair-production in  $p\bar{p}$  collisions. Extending the (modified) QGS model to these processes, allows us to test it, because in this case some (albeit, quite old) experimental data are available. Moreover, we use the fact that the ratios of the strong couplings of charmed and strange hadrons given in Table 1 have comparatively smaller uncertainties, than the individual couplings, because the same nucleon DA's are used in the sum rules in both cases of charmed and strange hadrons. Hence, we can constrain the couplings of strange hadrons by fitting the model cross

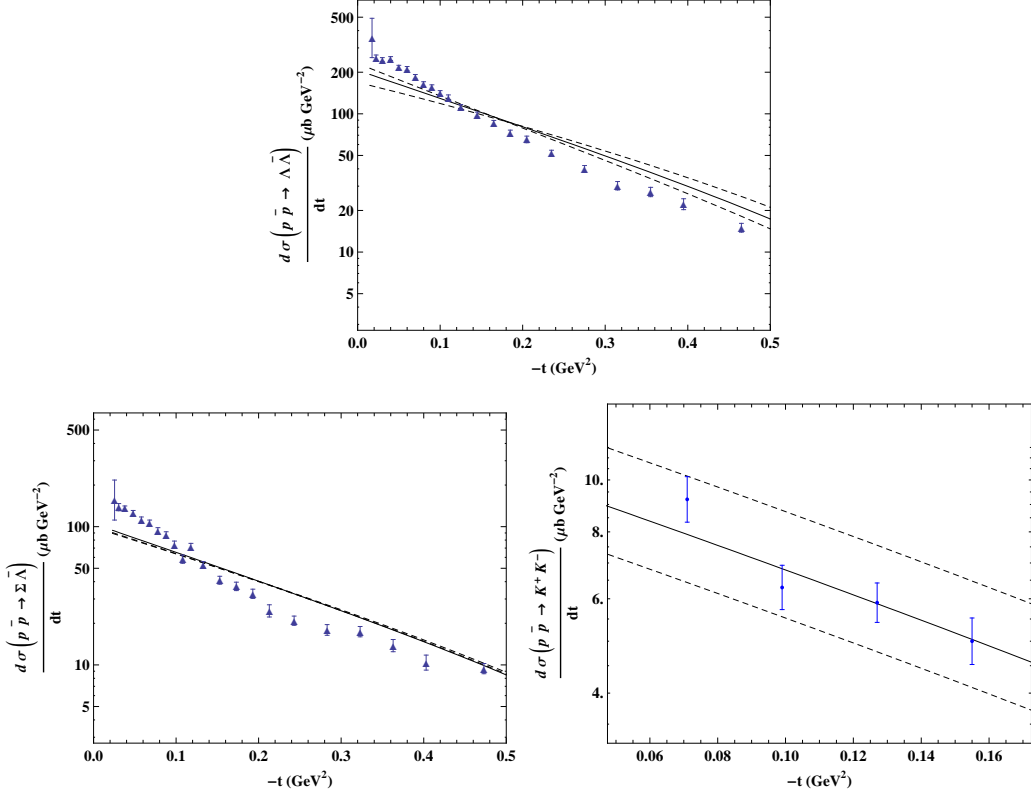


Figure 4: *Differential cross sections of  $p\bar{p} \rightarrow \Lambda\bar{\Lambda}$  and  $p\bar{p} \rightarrow \Sigma\bar{\Lambda}$  at  $p_{lab} = 6$  GeV, and  $p\bar{p} \rightarrow K^+K^-$  at  $p_{lab} = 4$  GeV. The data points are from [26, 27]. The solid curves are given by QGS model, with the ratio of tensor to vector strong couplings from LCSR (dashed curves indicate the uncertainties) and the vector strong couplings fitted to the measured cross-section normalization.*

sections to experimental data and then use the calculated ratios of the couplings to reproduce the charm cross sections with smaller uncertainties.

Let us start with the process  $p\bar{p} \rightarrow \Lambda\bar{\Lambda}$ . Its cross section in the QGS model has the same form as (21), with the strong couplings  $g_{\Lambda N K^*}^{V,T}$ , the  $K^*$  Regge-trajectory and the absorption factor  $C_A^{(p\bar{p} \rightarrow \Lambda\bar{\Lambda})}$ . We first calculate the differential cross section  $\frac{d\sigma}{dt}(p\bar{p} \rightarrow \Lambda\bar{\Lambda})$ , without taking into account the absorption factor, and fit the slope of the  $t$ -dependence to the exponential form  $\exp(-L_R(s)|t|)$ . In this cross section we use the ratio of tensor and vector strong couplings,  $g_{\Lambda N K^*}^T/g_{\Lambda N K^*}^V$ , obtained from LCSR (see Table 1). The slope  $L_R$  is then used to calculate the absorption factor  $C_A^{(p\bar{p} \rightarrow \Lambda\bar{\Lambda})}$  as explained in App. B. Note that the overall normalization of the cross section depending on the vector strong coupling  $g_{\Lambda N K^*}^V$  does not play role in this determination. On the other hand, due to difference of the slopes  $L_R$  for the Regge amplitudes of strange and charmed hadron production

the resulting absorption factor turns out to be almost twice larger for  $p\bar{p} \rightarrow \Lambda\bar{\Lambda}$  than for  $p\bar{p} \rightarrow \Lambda_c\bar{\Lambda}_c$  at small  $t$  (see App. B), in accordance with the estimates in [2].

After inserting the calculated absorption factor in the differential cross section of  $p\bar{p} \rightarrow \Lambda\bar{\Lambda}$ , in Fig.4 we compare the latter with the data points [26] at  $p_{lab} = 6$  GeV and at small  $t$  where we expect the QGS model to work. Note that not only the Regge amplitude itself but also the absorption factor contribute to  $t$ -dependence, making it steeper. As can be seen from this figure, the agreement of the shape of the differential cross sections with the data is not very good, which can possibly be traced back to slightly oversimplified model of  $t$  dependence for this particular (not yet sufficiently large) energy in our model. Still in the integrated cross section which is our main interest here, we expect that the imperfection of the shape does not play an important role.

As a next step, we fit the overall normalization of the cross section to the data and obtain the interval of the vector strong coupling

$$|g_{\Lambda NK}^V| = 5.5_{-0.3}^{+0.2}, \quad (25)$$

which is within the broader interval of the LCSR prediction given in Table 1. After that, we combine the above estimate with the calculated ratio  $g_{\Lambda_c ND}^V/g_{\Lambda NK}^V$  (see Table 1) and estimate the vector coupling for the charm case  $|g_{\Lambda_c ND}^V| = 5.2_{-1.6}^{+1.9}$ , again in agreement with the interval of LCSR prediction. We use the above “rescaled” interval for  $g_{\Lambda_c ND}^V$  in obtaining the charmed baryon cross section (21), thereby decreasing the resulting uncertainty. Note that the ratio  $g_{\Lambda_c ND}^T/g_{\Lambda_c ND}^V$  is again taken from the LCSR prediction. The cross section of  $\Lambda_c$  pair production we are interested in is then calculated in two steps: first we fix the exponential slope  $L_R$  in order to obtain the absorption factor and second, include this factor in the cross section. To estimate the cross sections of  $p\bar{p} \rightarrow \Sigma_c\bar{\Lambda}_c, \bar{\Sigma}_c\Sigma_c$  and  $p\bar{p} \rightarrow \bar{D}^0 D^0$ , we use a similar procedure employing the available data on strange hadron pair production (see Fig. 4). In particular, fitting of the corresponding strong couplings yields  $|g_{\Sigma NK}^V| = 3.9_{-0.2}^{+0.1}$  and  $|g_{\Lambda NK}| = 13.9_{-0.7}^{+0.9}$ . The LCSR predictions for these couplings given in Table 1 are only marginally consistent with the above intervals. Note that the predictions of the potential model [20] with the scattering potentials obeying a (slightly broken)  $SU(3)_{fl}$  symmetry, for the same couplings are in a better agreement with the fitted values.

Differential cross sections of  $p\bar{p} \rightarrow \Lambda_c\bar{\Lambda}_c, \Sigma_c\bar{\Lambda}_c, \Sigma_c\bar{\Sigma}_c$  and  $p\bar{p} \rightarrow D\bar{D}$  are displayed in Fig. 5 as a function of  $t$  at  $p_{lab} = 15$  GeV. As expected, their slope is much smaller than in the case of strange hadron production. The integrated cross section  $\sigma(t_0, \Delta)$  of charmed baryon or meson pair-production is defined as the integral of the differential cross section over the region of small momentum transfers:  $\max\{t_1, t_0 - \Delta\} < t < t_0$ , where we adopt  $\Delta = 0.6$  GeV<sup>2</sup>. These cross sections plotted as a function of  $p_{lab}$  in the region accessible to  $\bar{P}ANDA$  are presented in Fig. 6. The summary of our results for the cross sections is also displayed in Table 4.

Let us emphasize that the uncertainties of the predicted cross sections are still quite large, even after we narrowed them using the strange hadron production data. Note that we only quote the uncertainties stemming from the LCSR estimates of the strong couplings. The QGS model itself has “systematical” uncertainties, which is difficult

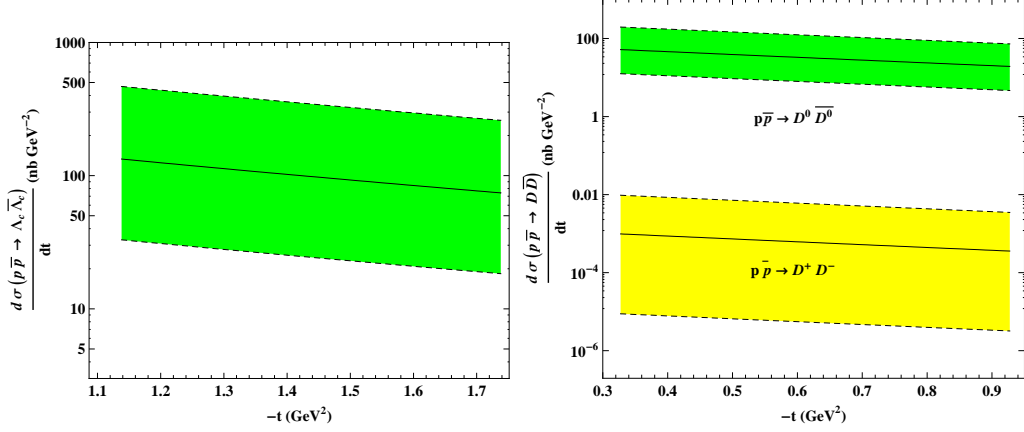


Figure 5: Differential cross sections of  $p\bar{p} \rightarrow \Lambda_c\bar{\Lambda}_c$ , and  $p\bar{p} \rightarrow D\bar{D}$  at  $p_{lab} = 15$  GeV calculated in QGS model. The dashed lines indicate the uncertainties caused by LCSR estimates of strong couplings.

to assess quantitatively, as it is the case for any phenomenological hadronic model not directly related to QCD. The predictive power of the model concerns mostly the ratios of cross sections, where the “intrinsic” uncertainties of the method to a large extent cancel. One important prediction concerns the suppression of  $\Sigma_c^-$  with respect to  $\Lambda_c^-$ -production cross section.

This suppression is more significant than predicted in [2] where simple relations based on the nonrelativistic quark-diquark model for these reactions are used

$$\frac{\sigma(p\bar{p} \rightarrow \Lambda_c\bar{\Lambda}_c)}{\sigma(p\bar{p} \rightarrow \Sigma_c\bar{\Lambda}_c)} = \frac{\sigma(p\bar{p} \rightarrow \Sigma_c\bar{\Lambda}_c)}{\sigma(p\bar{p} \rightarrow \Sigma_c\bar{\Sigma}_c)} = 3. \quad (26)$$

Our predictions for these ratios at  $p_{lab} = 15$  GeV are:

$$\frac{\sigma(p\bar{p} \rightarrow \Lambda_c\bar{\Lambda}_c)}{\sigma(p\bar{p} \rightarrow \Sigma_c\bar{\Lambda}_c)} = 5.1^{+1.0}_{-2.0}, \quad \frac{\sigma(p\bar{p} \rightarrow \Sigma_c\bar{\Lambda}_c)}{\sigma(p\bar{p} \rightarrow \Sigma_c\bar{\Sigma}_c)} = 4.6^{+0.9}_{-1.8}. \quad (27)$$

Due to the suppression of  $\Sigma_c$  couplings versus  $\Lambda_c$  couplings, also the  $D^0\bar{D}^0$  production cross section is expected to be significantly larger than the  $D^+\bar{D}^-$  one. It will be very interesting to test all these predictions experimentally.

## 5 Conclusion

In this paper we bring together the strong couplings of charmed and strange baryons, both predicted within one and the same QCD based method of LCSR. We have demonstrated that it is possible to avoid  $SU(4)_{fl}$  approximation. The relations between couplings are nontrivial because they stem from the nonperturbative dynamics which is quite different for heavy and light (also strange) quarks. The LCSR predictions for

channel	$\frac{d\sigma}{dt} _{t=t_0} (nb \text{ GeV}^{-2})$	$\sigma(t_0, \Delta)(nb)$
$p\bar{p} \rightarrow \Lambda_c \bar{\Lambda}_c$	130 (30 ÷ 470)	60 (15 ÷ 210)
$p\bar{p} \rightarrow \Sigma_c \bar{\Lambda}_c$	24 (5.0 ÷ 140)	12 (2.0 ÷ 70)
$p\bar{p} \rightarrow \Sigma_c \bar{\Sigma}_c$	5.0 (1.0 ÷ 45)	3.0 (0.4 ÷ 24)
$p\bar{p} \rightarrow D^0 \bar{D}^0$	52 (13 ÷ 200)	20 (5.0 ÷ 75)
$p\bar{p} \rightarrow D^+ \bar{D}^-$	< 0.01	< 0.01

Table 4: *Differential and integrated cross sections with  $\Delta = 0.6 \text{ GeV}^2$  for charmed hadron production at  $p_{lab} = 15 \text{ GeV}$ .*

strong couplings can be significantly improved in future by calculating radiative gluon corrections and taking into account soft gluon components of the nucleon DA's.

The main task of this paper is to estimate the charm production cross sections in  $p\bar{p}$  collisions. For that purpose we have selected the most (in our opinion) ‘‘QCD-friendly’’ model of hadronic reactions, that is, the Kaidalov’s QGS model. This approach has revealed itself as a very useful tool for hadronic reactions with different flavours, also for inclusive production of hadrons. In this paper we used a more detailed description of binary processes with baryons in terms of helicity amplitudes and employed the strong couplings of initial protons and final charmed baryons (mesons) with the intermediate charmed mesons (baryons) calculated from LCSR.

Strictly speaking, the QGS model is applicable only at sufficiently large energies, beyond the upper limit of the  $\bar{P}ANDA$  energy region. Hence the cross sections calculated here can only be considered as an order of magnitude estimates, also because the model is only valid at small momentum transfers and the absorption factor is only taken in the first approximation. Still the relations between cross sections are less influenced by the uncertainties and are almost independent of the absorption factors. In future, the model adopted in this paper can be developed further, taking into account of the subleading Regge trajectories and a more elaborated absorption ansatz.

Finally, turning to the comparison of our results with the charm-production estimates in the literature, we observe that our prediction for the dominant  $\Lambda_c \bar{\Lambda}_c$  production is (within estimated uncertainties) consistent with the one obtained in the original QGS model [2]:  $\sigma(p\bar{p} \rightarrow \Lambda_c \bar{\Lambda}_c) \simeq 100 \text{ nb}$ , at  $p_{lab} = 15 \text{ GeV}$ , whereas the predictions for the ratios of cross sections obtained here and in [2] differ. For example, we do not exclude a larger charmed meson cross section than  $\sigma(p\bar{p} \rightarrow D^0 \bar{D}^0) \simeq 5 \text{ nb}$  predicted in [2].



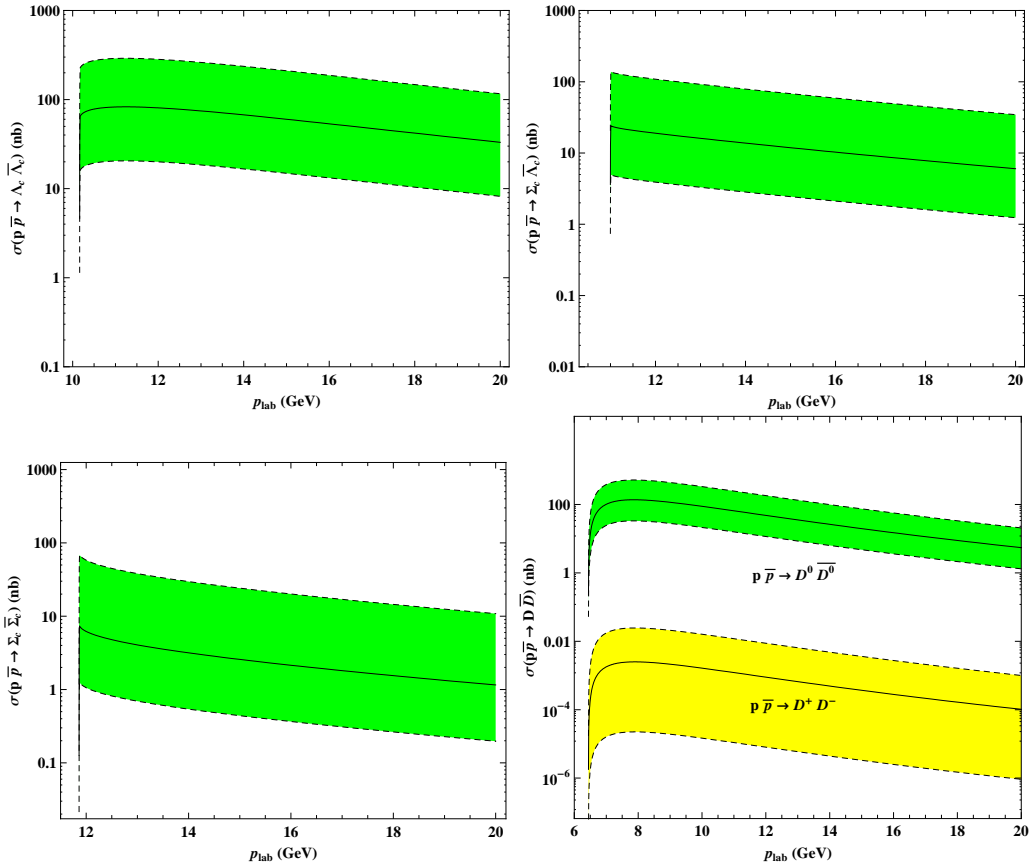


Figure 6: The integrated cross sections  $\sigma(t_0, \Delta)$  of charmed baryon and meson pair production in  $p\bar{p}$  collisions in QGS model. The dashed lines indicate the uncertainties introduced by the strong couplings obtained from LCSR.

A model of exclusive charm production cross sections based on the QGS and Regge-poles can be found in [3], where the  $SU(4)_{fl}$  symmetry is used and a different form of the cross section is adopted, adding a  $t$ -dependent dipole “residual factor”. Numerically, our predicted intervals for the differential cross sections at  $t_0$  turn out to be larger than the ones in [3].

The other models in the literature are based on radically different approaches. E.g., in [8] a hadronic baryon-antibaryon potential derived from the coupled channel approach is used, predicting the cross section of  $\Lambda_c\bar{\Lambda}_c$  production up to a few  $\mu b$  near the threshold, i.e., much larger than obtained here. On the opposite side are the typically smaller cross sections obtained from perturbative approaches, such as the inclusive charm production estimate in the parton model [7] and the approach [6] to  $p\bar{p} \rightarrow \Lambda_c\bar{\Lambda}_c$  employing distribution amplitudes of initial and final baryons.

Concluding, this paper contains an attempt to apply QCD predictions for hadronic strong couplings to the models of exclusive hadronic reactions. Our estimates for charm production cross sections contain rather large uncertainties. Still even the lower limit of

the cross sections predicted here allows one to expect an appreciable number of charmed baryons and mesons produced at  $\bar{P}ANDA$ . We look forward to other applications of the strong couplings presented in this paper and their future improvements.

## Acknowledgments

This work is supported by the German Ministry for Education and Research (BMBF) under contract 06SI9192. T.M. also thanks A. Titov for a discussion on the subject of the paper.

## Appendix A: Helicity amplitudes

The helicity amplitudes of  $\bar{p}p \rightarrow \bar{\Lambda}_c \Lambda_c$  scattering via  $D^*$  meson exchange are obtained from the initial invariant scattering amplitude

$$H(\lambda_1 \lambda_2; \lambda_3 \lambda_4) = \frac{1}{m_{D^*}^2 - t} \bar{u}_{\Lambda_c}(p_3, \lambda_3) \left[ g_{\Lambda_c N D^*}^V \not{\epsilon} + i \frac{g_{\Lambda_c N D^*}^T}{m_{\Lambda_c} + m_N} \sigma_{\mu\nu} \epsilon^\mu q^\nu \right] u_N(p_1, \lambda_1) \bar{v}_{\bar{N}}(p_2, \lambda_2) \left[ g_{\Lambda_c N D^*}^V \not{\epsilon}^* + i \frac{g_{\Lambda_c N D^*}^T}{m_{\Lambda_c} + m_N} \sigma_{\rho\tau} \epsilon^{*\rho} q^\tau \right] v_{\Lambda_c}(p_4, \lambda_4), \quad (28)$$

where the baryon bispinors are distinguished by their indices so that  $(p_1, \lambda_1)$ ,  $(p_2, \lambda_2)$ ,  $(p_3, \lambda_3)$  and  $(p_4, \lambda_4)$  are the four-momenta and helicities of the proton, antiproton,  $\Lambda_c$  and  $\bar{\Lambda}_c$  respectively;  $\epsilon_\mu$  is the polarization vector of the virtual  $D^*$  meson. Generally, there are 16 different helicity amplitudes for  $\bar{p}p \rightarrow \bar{\Lambda}_c \Lambda_c$  process, only six of them are independent due to symmetries [28].

In the c.m. frame of proton-antiproton pair we choose the  $x, z$  plane for the process, and the 3-momentum of proton in the  $z$  direction, so that the 3-momentum of  $\Lambda_c$  has the angular coordinates  $(\theta, \varphi = 0)$ . Then the kinematics is as follows:

$$\begin{aligned} p_1 &= \frac{1}{2}(\sqrt{s}, 0, 0, \sqrt{s - 4m_N^2}), & p_2 &= \frac{1}{2}(\sqrt{s}, 0, 0, -\sqrt{s - 4m_N^2}), \\ p_3 &= \frac{1}{2}(\sqrt{s}, \sqrt{s - 4m_{\Lambda_c}^2} \sin \theta, 0, \sqrt{s - 4m_{\Lambda_c}^2} \cos \theta), \\ p_4 &= \frac{1}{2}(\sqrt{s}, -\sqrt{s - 4m_{\Lambda_c}^2} \sin \theta, 0, -\sqrt{s - 4m_{\Lambda_c}^2} \cos \theta) \end{aligned} \quad (29)$$

Summing over the polarization of  $D^*$  meson:

$$\sum_{\lambda=1,2,3,4} \epsilon^\mu(q, \lambda) \epsilon^{\nu*}(q, \lambda) = -g^{\mu\nu} + \frac{q^\mu q^\nu}{m_{D^*}^2}, \quad (30)$$

and substituting explicitly the bispinors with various helicities in the chosen frame we obtain rather bulky expressions of helicity amplitudes, which however greatly simplify in

the limit of large  $s$  where we compare them with the Regge amplitudes. The six helicity amplitudes are:

$$\begin{aligned}
H(++ , ++ ) &= \frac{s}{t - m_{D^*}^2} 2(g_{\Lambda_c ND^*}^V)^2, \\
H(+ - , ++ ) &= \frac{s}{t - m_{D^*}^2} \frac{2\sqrt{-t} g_{\Lambda_c ND^*}^V g_{\Lambda_c ND^*}^T}{m_{\Lambda_c} + m_N}, \\
H(++ , - + ) &= -\frac{s}{t - m_{D^*}^2} \frac{2\sqrt{-t} g_{\Lambda_c ND^*}^V g_{\Lambda_c ND^*}^T}{m_{\Lambda_c} + m_N}, \\
H(- - , ++ ) &= -\frac{s}{t - m_{D^*}^2} \frac{2t (g_{\Lambda_c ND^*}^T)^2}{(m_{\Lambda_c} + m_N)^2}, \\
H(- + , - + ) &= \frac{s}{t - m_{D^*}^2} 2(g_{\Lambda_c ND^*}^V)^2, \\
H(+ - , - + ) &= \frac{s}{t - m_{D^*}^2} \frac{2t (g_{\Lambda_c ND^*}^T)^2}{(m_{\Lambda_c} + m_N)^2}.
\end{aligned} \tag{31}$$

It is clear that in the large  $s$  limit only three helicity amplitudes are independent. The amplitudes can be related to each other through the following relations:

$$\begin{aligned}
H(-\lambda_1 - \lambda_2; -\lambda_3 - \lambda_4) &= (-1)^{\lambda_1 - \lambda_2 - \lambda_3 + \lambda_4} H(\lambda_1 \lambda_2; \lambda_3 \lambda_4), \\
H(\lambda_2 \lambda_1; \lambda_4 \lambda_3) &= (-1)^{\lambda_1 - \lambda_2 - \lambda_3 + \lambda_4} H(\lambda_1 \lambda_2; \lambda_3 \lambda_4),
\end{aligned} \tag{32}$$

following from the parity and charge-conjugation invariance.

## Appendix B: Absorption factor

Here we derive the absorption factor  $C_A(s, t)$ , multiplying the cross section. The absorption is generated by the (quasi) elastic rescattering of the initial proton and antiproton as well as of the final hadron pair, both are approximated by the pomeron exchange [2]. Here we make a simplifying assumption that the elastic rescattering amplitudes dominate, they do not change the helicities and are the same in the initial and final states, independent of the flavour content of the latter.

Consider a process  $p\bar{p} \rightarrow B\bar{B}$  with generic  $B$  hadrons in the final-state. The amplitude in QGS model, having the form (18) has predominantly exponential behavior at small  $t$ , the main source of it is the Regge-pole factor  $(s/s_0)^{\alpha(t)}$ . Therefore, the  $p\bar{p} \rightarrow B\bar{B}$  amplitude can be cast in the exponential form

$$T_R(s, t) = f_R(s) \exp\left(-\frac{L_R}{2}|t|\right). \tag{33}$$

We then switch to the impact parameter representation, where the 2-dimensional vector  $\vec{b}$  is conjugate to the transverse momentum transfer  $\vec{q}_\perp$ :

$$T_R(s, b) = \int T_R(s, t) \exp(i\vec{q}_\perp \cdot \vec{b}) \frac{d\vec{q}_\perp}{2\pi}, \tag{34}$$

and at high energies  $t \equiv q^2 \simeq -|\vec{q}|^2$ . The angular integration yields:

$$T_R(s, b) = \frac{1}{2} \int_0^\infty d|t| J_0(\sqrt{|t|}b) T_R(s, -|t|), \quad (35)$$

where  $J_0$  is the Bessel function and  $b = |\vec{b}|$ . Substituting the exponential representation (33) in the above integral, and integrating over  $t$  we obtain

$$T_R(s, b) = \frac{f_R(s)}{L_R} \exp\left(-\frac{b^2}{2L_R}\right). \quad (36)$$

The rescattering in the initial and final state is dominated by the pomeron amplitude  $T_P(s, t)$  which is predominantly imaginary and has an exponential form in the momentum transfer  $T_P(s, t) = T_P(s, 0) \exp(-L_P|t|/2)$ . The forward-scattering amplitude is expressed via total  $p\bar{p}$  cross section using the optical theorem:  $\text{Im}T_P(s, 0) = 2p^* \sqrt{s} \sigma_{p\bar{p}}^{\text{tot}}(s)$ , where  $p^*$  is the 3-momentum in the c.m. system of the  $p\bar{p}$  collision. Hence one obtains for the pomeron-mediated elastic rescattering amplitude:

$$T_P(s, t) = 2ip^* \sqrt{s} \sigma_{p\bar{p}}^{\text{tot}}(s) \exp(-L_P|t|/2). \quad (37)$$

Employing the same Fourier-transformation to the impact parameter space as in (34), it is easy to get the impact parameter representation for this amplitude:

$$T_P(s, b) = \frac{2ip^* \sqrt{s} \sigma_{p\bar{p}}^{\text{tot}}(s)}{L_P} \exp\left(-\frac{b^2}{2L_P}\right). \quad (38)$$

The absorption contribution added to the initial Reggeon amplitude in the  $b$  space yields:

$$T(s, b) = T_R(s, b) \left[ 1 + i \frac{T_P(s, b)}{8\pi p^* \sqrt{s}} \right] = T_R(s, b) \left[ 1 - \chi(s, b) \right], \quad (39)$$

where

$$\chi(s, b) = \frac{\sigma_{p\bar{p}}^{\text{tot}}(s)}{4\pi L_P} \exp\left(-\frac{b^2}{2L_P}\right), \quad (40)$$

and the normalization factor multiplying  $T_P$  corresponds to the convention of impact parameter representation adopted in [2]. Substituting (36) in (39) and performing the inverse Fourier transformation to the  $t$ -dependent amplitude we finally obtain:

$$T(s, t) = T_R(s, t) \left[ 1 - \frac{\sigma_{p\bar{p}}^{\text{tot}}(s)}{4\pi(L_P + L_R)} \exp\left(\frac{L_R^2|t|}{2(L_P + L_R)}\right) \right]. \quad (41)$$

This expression takes into account absorption in the amplitude in the first approximation. To obtain  $C_A(s, t)$  one simply has to square the expression in brackets multiplying  $T_R(s, t)$  in the above. At high energies this effect should be resummed (exponentiated), however at small  $t$ 's we are considering here the resummation effects, as we checked numerically, are small, so that the first approximation for  $C_A$  is sufficient.

For the numerical evaluation of the absorption factor in (41), the data on  $\sigma_{p\bar{p}}^{tot}(s)$  in a parameterized form are taken from [21], so that  $\sigma_{p\bar{p}}^{tot}(s)$  changes from 52.5 mb to 47.9 mb in the interval  $p_{lab} = 10$  GeV to 20 GeV. The slope of the pomeron mediated elastic  $p\bar{p}$  scattering is taken from [29], e.g.,  $L_P = 12.1$  GeV<sup>-2</sup> at  $p_{lab} = 15$  GeV. Finally, the slopes of Regge-pole amplitudes fitted to the exponential form (33) are (in units GeV<sup>-2</sup>):  $L_R = 2.6$  ( $p_{lab} = 6$  GeV) and 2.5 ( $p_{lab} = 4$  GeV) for  $p\bar{p} \rightarrow \Lambda\bar{\Lambda}$ ,  $\Sigma\bar{\Lambda}$  and  $K^+K^-$ , respectively. For  $p\bar{p} \rightarrow \Lambda_c\bar{\Lambda}_c$ ,  $\Sigma_c\bar{\Lambda}_c$ ,  $\Sigma_c\bar{\Sigma}_c$ ,  $D\bar{D}$ , the corresponding slopes are  $L_R = 0.6, 0.4, 0.2, 1.2$  ( $p_{lab} = 15$  GeV), respectively. For numerical illustration, we quote the absorption factors calculated at the same energy  $p_{lab} = 15$  GeV and at  $t = t_0$  for strange and charmed baryon production:  $C_A^{(p\bar{p} \rightarrow \Lambda\bar{\Lambda})} = 0.09$  and  $C_A^{(p\bar{p} \rightarrow \Lambda_c\bar{\Lambda}_c)} = 0.04$ . These values are in agreement with ( $t$ -averaged) values presented in [2] and indicate a strong absorption effect on one hand and a large difference between this effect for strange and charmed baryons.

## References

- [1] U. Wiedner, Prog. Part. Nucl. Phys. **66** (2011) 477.
- [2] A. B. Kaidalov and P. E. Volkovitsky, Z. Phys. C **63** (1994) 517.
- [3] A. I. Titov and B. Kampfer, Phys. Rev. C **78**, 025201 (2008);
- [4] A. I. Titov and B. Kampfer, arXiv:1105.3847 [hep-ph].
- [5] P. Kroll, B. Quadder and W. Schweiger, Nucl. Phys. B **316** (1989) 373.
- [6] A. T. Goritschnig, P. Kroll and W. Schweiger, Eur. Phys. J. A **42** (2009) 43.
- [7] E. Braaten and P. Artoisenet, Phys. Rev. D **79**, 114005 (2009).
- [8] J. Haidenbauer and G. Krein, Phys. Lett. B **687**, 314 (2010).
- [9] J. Haidenbauer and G. Krein, Few Body Syst. **50** (2011) 183.
- [10] B. Kerbikov and D. Kharzeev, Phys. Rev. D **51** (1995) 6103.
- [11] A. Khodjamirian, C. Klein, T. Mannel and Y. M. Wang, JHEP **09** (2011) 106.
- [12] A. B. Kaidalov and P. E. Volkovitsky, Sov. J. Nucl. Phys. **35** (1982) 909 [Yad. Fiz. **35** (1982) 1556];
- [13] A. B. Kaidalov and P. E. Volkovitsky, Sov. J. Nucl. Phys. **35** (1982) 720 [Yad. Fiz. **35** (1982) 1231];
- [14] A. B. Kaidalov, Surveys High Energ. Phys. **13** (1999) 265.
- [15] A. B. Kaidalov and A. V. Nogteva, Sov. J. Nucl. Phys. **47** (1988) 321 [Yad. Fiz. **47** (1988) 505].

- [16] V. Braun, R. J. Fries, N. Mahnke and E. Stein, Nucl. Phys. B **589** (2000) 381 [Erratum-ibid. B **607** (2001) 433];
- [17] V. M. Braun, A. Lenz and M. Wittmann, Phys. Rev. D **73** (2006) 094019;
- [18] A. Lenz, M. Gockeler, T. Kaltenbrunner and N. Warkentin, Phys. Rev. D **79**, 093007 (2009).
- [19] Y. L. Liu and M. Q. Huang, Nucl. Phys. A **821** (2009) 80.
- [20] V. G. J. Stoks and T. A. Rijken, Phys. Rev. C **59**, 3009 (1999).
- [21] K. Nakamura *et al.* [Particle Data Group], J. Phys. G **37** (2010) 075021.
- [22] V. M. Belyaev, V. M. Braun, A. Khodjamirian and R. Rückl, Phys. Rev. D **51** (1995) 6177.
- [23] A. Khodjamirian, R. Rückl, S. Weinzierl and O. I. Yakovlev, Phys. Lett. B **457** (1999) 245.
- [24] S. Ahmed *et al.* [CLEO Collaboration], Phys. Rev. Lett. **87** (2001) 251801.
- [25] A. Khodjamirian and A. G. Oganesian, Phys. Atom. Nucl. **56** (1993) 1720 [Yad. Fiz. **56** (1993) 172].
- [26] H. Becker *et al.* [CERN-Munich Collaboration], Nucl. Phys. B **141** (1978) 48.
- [27] A. Brabson *et al.*, Phys. Lett. B **42** (1972) 287.
- [28] C. Bourrely, J. Soffer and E. Leader, Phys. Rept. **59** (1980) 95.
- [29] V. A. Okorokov, arXiv:0811.3849 [hep-ph].